Supporting Information

Screening of transition metal single-atom catalysts supported by a WS_2 monolayer for electrocatalytic nitrogen reduction reaction: insights from activity trend and descriptor

Renyi Li[†] and Wei Guo[†,*]

[†] Key Lab of Advanced Optoelectronic Quantum Architecture and Measurement (MOE), School of Physics, Beijing Institute of Technology, Beijing 100081, China.
*Corresponding author

Note

Hydrogen evolution reaction (HER) is a competitive reaction of nitrogen reduction reaction (NRR), which commonly reduces the Faraday efficiency (FE) of NRR. The hydrogen adsorption free energy, ΔG(*H), is computed by using the equation as follows:

$$\Delta G(*H) = \Delta E(*H) + \Delta ZPE - T\Delta S$$

where ΔE(*H) is the adsorption energy of H adatom adsorbed on the TM@WS_2 via DFT calculations. ΔZPE and ΔS are the difference in the zero-point energy and entropy between the adsorbed H adatom and the gaseous H_2. ΔS can be calculated as $-1/2S_0$ (S_0 is the entropy of H_2 in the gas phase at standard conditions) due to the entropy of hydrogen in adsorbed state is negligible. The above equation can be calculated roughly by ΔG(*H) = ΔE(*H) + 0.24 eV when T = 300 K[1].

We estimate the FE of NRR by Boltzmann distribution and the formula of FE of NRR can be expressed as:

$$f_{NRR} = \frac{1}{1 + e^{-\frac{\Delta G}{k_B T}}} \times 100\%$$

where ΔG is Gibbs free energy difference between potential determining step (PDS) of HER and NRR, k_B is the Boltzmann constant and T is the room temperature[2, 3].

The computational details of Microkinetic modeling

The elementary reaction steps are shown as follows:

step 1: * + N_2(g) = *N_2

step 2: *N_2 + (H^++e^-) = *NNH

step 3: *NNH + (H^++e^-) = *NNH_2

step 4: *NNH_2 + (H^++e^-) = *NNH_3

step 5: *NNH_3 = *N + NH_3(g)

step 6: *N + (H^++e^-) = *NH

step 7: *NH + (H^++e^-) = *NH_2

step 8: *NH_2 + (H^++e^-) = *NH_3

step 9: *NH_3 = * + NH_3(g)

where * represents an active site.

The rate constant and equilibrium constant of an elementary reaction step are calculated by using transition state theory and thermodynamic equilibrium.

For the N_2 adsorption step (step 1), the rate constant ($\boldsymbol{k_1}$) is given by the collision theory:

$$k_1 = \frac{\sigma A P^O}{\sqrt{2\pi m k_B T}} exp(-\frac{\Delta E_{1,barrier}}{k_B T})$$

where σ is the sticking coefficient, A is the surface area of an active site and we estimate this parameter to be 1×10^{-20} m^2. P^o is the standard pressure (1 bar), m is the mass of the adsorbate, and $\Delta E_{1,\,barrier}$ is the activation energy of N_2 adsorption. k_B is the Boltzmann constant and T is the temperature. The sticking coefficient is set to 1, and N_2 adsorption is taken to be barrierless[4].

The equilibrium constant of the N_2 adsorption step, $\boldsymbol{K_1}$:

$$K_1 = exp(-\frac{\Delta G_1}{k_B T})$$

where ΔG_1 is the Gibbs free energy of N_2 adsorption at standard pressure. The free energies for gas molecules are estimated by using the ideal gas approximation, which considers the vibrational, rotational, and translational contributions, while the free energies for surface adsorbates are approximated using the harmonic approximation that treats all degrees of freedom as vibrational modes.

For the reserved reaction of N_2 adsorption, i.e., N_2 desorption, the formula for rate constant $\boldsymbol{k_{-1}}$ is as follows:

$$k_{-1} = k_1/K_1$$

For the NH_3 desorption step, the solving process of the rate constant is analogous to the adsorption process.

For all electrochemical steps, the rate constant ($\boldsymbol{k_i}$) of forward reaction:

$$k_i = \frac{k_B T}{h} exp(-\frac{\Delta G_{i,TS}}{k_B T})$$

The equilibrium constants ($\boldsymbol{K_i}$):

$$K_i = exp(-\frac{\Delta G_i}{k_B T})$$

Rate constant of the reversed reaction ($\boldsymbol{k_{-i}}$):

$$k_{-i} = k_i/K_i$$

where $\Delta G_{i,TS}$ is the calculated free energy barrier of the step *i* by using CI-NEB method. ΔG_i is the free energy change of the step *i*.

The reaction rate ($\boldsymbol{r_i}$) of the step *i* is computed by using the law of mass action[5]:

$$r_i = k_{f,i} \prod_j \alpha^{v_{i,j}} - k_{r,j} \prod_j \alpha^{v_{i,j}}$$

where α is the activity of the species, such as pressure for gas, concentration for solvated species, and coverage for surface species. $v_{i,j}$ is the stoichiometric coefficient for species j of the step *i*.

The rate equations are shown as follows:

(1) $r_1 = k_1 \theta^* pN_2(g) - k_{-1} \theta^* N_2$

(2) $r_2 = k_2\ \theta^*N_2\ p(H^+) - k_{-2}\ \theta^*NNH$

(3) $r_3 = k_3\ \theta^*NNH\ p(H^+) - k_{-3}\ \theta^*NNH_2$

(4) $r_4 = k_4\ \theta^*NNH_2\ p(H^+) - k_{-4}\ \theta^*NNH_3$

(5) $r_5 = k_5\ \theta^*NNH_3 - k_{-5}\ \theta^*N\ pNH_3(g)$

(6) $r_6 = k_6\ \theta^*N\ p(H^+) - k_{-6}\ \theta^*NH$

(7) $r_7 = k_7\ \theta^*NH\ p(H^+) - k_{-7}\ \theta^*NH_2$

(8) $r_8 = k_8\ \theta^*NH_2\ p(H^+) - k_{-8}\ \theta^*NH_3$

(9) $r_9 = k_9\ \theta^*NH_3 - k_{-9}\ \theta^*\ pNH_3(g)$

where $pN_2(g)$, $p(H^+)$, $pNH_3(g)$ are the partial pressures of N_2, H^+, NH_3. We refer to recent published works to set these partial pressures[6-11]. The parameters setting are shown as follows:

$pN_2(g) = 0.005 + 0.25\times P$

$p(H^+) = 3\times pN_2(g)$

$pNH_3(g) = 0.2\times pN_2$

$P \in [0, 100]$ (P in bar)

The H^+ : N_2 ratio is fixed at 3 and the ammonia conversion ratio is set to 10%[12].

The step 2 is rate-determining step (RDS) and the rates of all other steps equal to 0:

(10) $r_1 = r_3 = r_4 = r_5 = r_6 = r_7 = r_8 = r_9 = 0$

Coverage of all the reaction species is equal to 1.

(11) $\theta^* + \theta^*N_2 + \theta^*NNH + \theta^*NNH_2 + \theta^*NNH_3 + \theta^*N + \theta^*NH + \theta^*NH_2 + \theta^*NH_3 = 1$

The rate equations (1-9) combined with (10) and (11) can be solved analytically given pressure P ($P \in [0, 100]$ in bar) and temperature ($T \in [300, 1000]$ in K). The reaction rate ($\boldsymbol{r_2}$) of the step 2 can be obtained, which gives the turnover frequency (TOF).

Considering the reaction rate can be regulated by the electrode potential (U)[13], the rate constant ($\boldsymbol{k_i}$) and equilibrium constant ($\boldsymbol{K_i}$) of an electrochemical step can be written as:

$$k_i = \frac{k_B T}{h} exp(-\frac{\Delta G_{i,TS}}{k_B T}) exp(-\frac{e\beta(U - U_i)}{k_B T})$$

$$K_i = exp(-\frac{e(U-U_i)}{k_B T})$$

where U_i is the reversible potential of step *i*, which can be deduced by $U_i = -\Delta G_i / e$. β is the symmetric factor taken as 0.5.

Rate constant of the reversed reaction (k_{-i}):

$$k_{-i} = k_i / K_i$$

The time-dependent concentration is described as:

$$\frac{\partial \theta_j}{\partial t} = \sum_i v_{i,j} r_i$$

The rate equations of each species are as follows:

(12) $\partial\theta^*/\partial t = -k_1\,\theta^*\,pN_2(g) + k_{-1}\,\theta^*N_2 + k_9\,\theta^*NH_3 - k_{-9}\,\theta^*\,pNH_3(g)$

(13) $\partial\theta^*N_2/\partial t = k_1\,\theta^*\,pN_2(g) - k_{-1}\,\theta^*N_2 - k_2\,\theta^*N_2 + k_{-2}\,\theta^*NNH$

(14) $\partial\theta^*NNH/\partial t = k_2\,\theta^*N_2 - k_{-2}\,\theta^*NNH - k_3\,\theta^*NNH + k_{-3}\,\theta^*NNH_2$

(15) $\partial\theta^*NNH_2/\partial t = k_3\,\theta^*NNH - k_{-3}\,\theta^*NNH_2 - k_4\,\theta^*NNH_2 + k_{-4}\,\theta^*NNH_3$

(16) $\partial\theta^*NNH_3/\partial t = k_4\,\theta^*NNH_2 - k_{-4}\,\theta^*NNH_3 - k_5\,\theta^*NNH_3 + k_{-5}\,\theta^*N\,pNH_3(g)$

(17) $\partial\theta^*N/\partial t = k_5\,\theta^*NNH_3 - k_{-5}\,\theta^*N\,pNH_3(g) - k_6\,\theta^*N + k_{-6}\,\theta^*NH$

(18) $\partial\theta^*NH/\partial t = k_6\,\theta^*N - k_{-6}\,\theta^*NH - k_7\,\theta^*NH + k_{-7}\,\theta^*NH_2$

(19) $\partial\theta^*NH_2/\partial t = k_7\,\theta^*NH - k_{-7}\,\theta^*NH_2 - k_8\,\theta^*NH_2 + k_{-8}\,\theta^*NH_3$

(20) $\partial\theta^*NH_3/\partial t = k_8\,\theta^*NH_2 - k_{-8}\,\theta^*NH_3 - k_9\,\theta^*NH_3 + k_{-9}\,\theta^*\,pNH_3(g)$

The partial pressure of N_2 in the catalyst-electrolyte interface is set to 1.0×10^{-5} bar. We refer to the previous works[13, 14] to estimate the partial pressure of N_2. The partial pressure of NH_3 is 0.2 times that of N_2.

The rate equations (12-20) combined with (11) can be numerically solved at steady state. The coverage of species and TOF vary with the electrode potential U. The current density (j) can be deduced by the formula:

$$j = e\rho TOF_e$$

where ρ is the density of active site of TM@WS_2. Here we use a 4×4×1 supercell of

WS_2 and only one TM is anchored on the support. The lattice constant of 4×4×1 WS_2 is 12.61 Å and the calculated ρ is equal to $1/(1.38 \times 10^{-14})$ cm^{-2}. Then, we can simulate the polarization curves of NRR.

Table S1. The zero-point energy vibration and entropy contribution of the adsorbed species during NRR on Re@WS_2. (T = 298.15 K)

Adsorbed species	ZPE	TS
***N**	0.08	0.07
***NH**	0.36	0.10
***NH_2**	0.66	0.09
***NH_3**	1.03	0.18
***NN**	0.21	0.15
***NNH**	0.48	0.17
***NNH_2**	0.81	0.19
***NHNH**	0.82	0.14
***$NHNH_2$**	1.13	0.15
***NH_2NH_2**	1.49	0.25

Table S2. The zero-point energy vibration and entropy contribution of the adsorbed species during NRR on Os@WS_2. (T = 298.15 K)

Adsorbed species	ZPE	TS

***N**	0.08	0.07
***NH**	0.35	0.10
***NH_2**	0.68	0.12
***NH_3**	1.03	0.17
***NN**	0.21	0.16
***NNH**	0.48	0.18
***NNH_2**	0.80	0.21
***NHNH**	0.83	0.19
***$NHNH_2$**	1.15	0.20
***NH_2NH_2**	1.50	0.22

Table S3. The zero-point energy vibration and entropy contribution of the adsorbed species during NRR on Ir@WS_2. (T = 298.15 K)

Adsorbed species	ZPE	TS
***N**	0.08	0.07
***NH**	0.33	0.11
***NH_2**	0.69	0.11
***NH_3**	1.03	0.14
***NN**	0.21	0.17
***NNH**	0.47	0.14
***NNH_2**	0.79	0.21
***NHNH**	0.83	0.19
***$NHNH_2$**	1.15	0.14
***NH_2NH_2**	1.50	0.19

Table S4. The free energy change ΔG (eV) of potential limiting step (PDS) of NRR and HER and Faraday efficiency of NRR (f_{NRR}) on various TM@WS_2.

TM@WS_2	ΔGmax(NRR)	ΔG(*H)	f_{NRR}
Sc	0.79	0.34	3.04×10^{-6}
Ti	0.75	0.34	1.42×10^{-5}
V	0.86	0.06	4.34×10^{-12}
Cr	0.70	0.16	9.55×10^{-8}
Mn	0.81	0.19	4.40×10^{-9}
Fe	0.94	0.06	2.00×10^{-13}
Co	0.98	0.25	6.40×10^{-11}
Ni	1.84	0.67	2.86×10^{-18}
Cu	1.21	0.43	9.36×10^{-12}
Y	0.76	0.31	3.04×10^{-6}
Zr	0.81	0.54	3.09×10^{-3}
Nb	0.61	0.27	2.09×10^{-4}
Mo	0.54	0.28	4.54×10^{-3}
Tc	0.46	0.20	4.54×10^{-3}
Ru	0.68	0.23	3.04×10^{-6}

Rh	1.02	0.33	2.98×10^{-10}
Pd	1.87	0.81	1.97×10^{-16}
Lu	0.73	0.18	6.50×10^{-8}
Ta	1.18	0.83	1.42×10^{-4}
Re	0.44	0.79	100
Os	0.38	0.55	99.86
Ir	0.69	0.78	96.96
Pt	1.72	0.07	2.75×10^{-26}

Hybrid functional (HSE06) testing

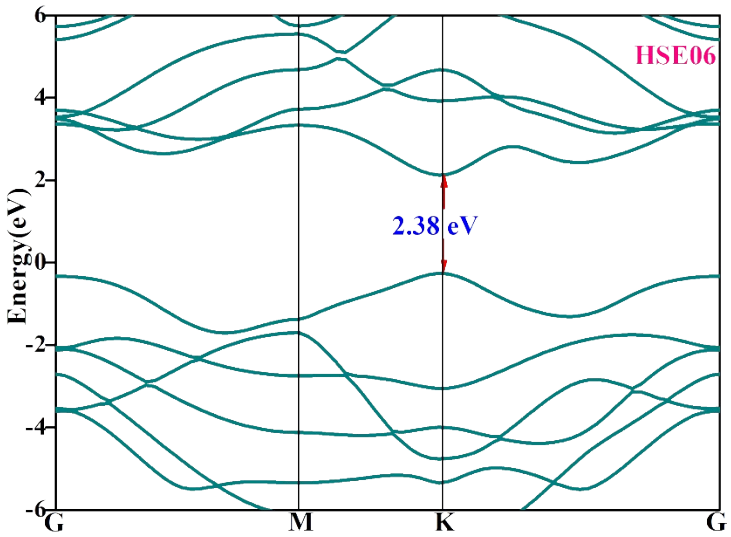

Figure S1 Calculated band structure of the pristine WS_2 monolayer via hybrid functional (HSE06).

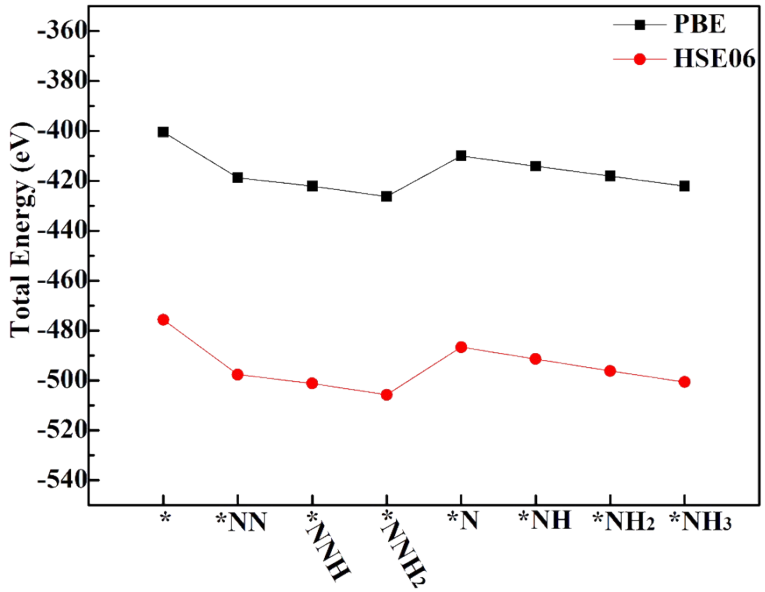

Figure S2 Calculated total energies of reaction intermediates on Os@WS_2 via PBE functional and hybrid functional (HSE06).

Solvent effect testing

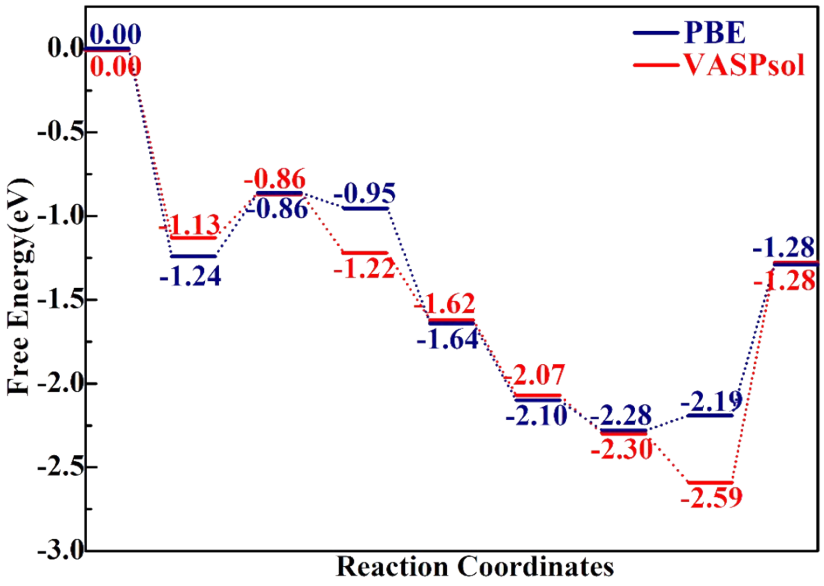

Figure S3 Calculated Gibbs free energies of reaction intermediates on Os@WS_2 via PBE functional

and PBE functional with solvation effect.

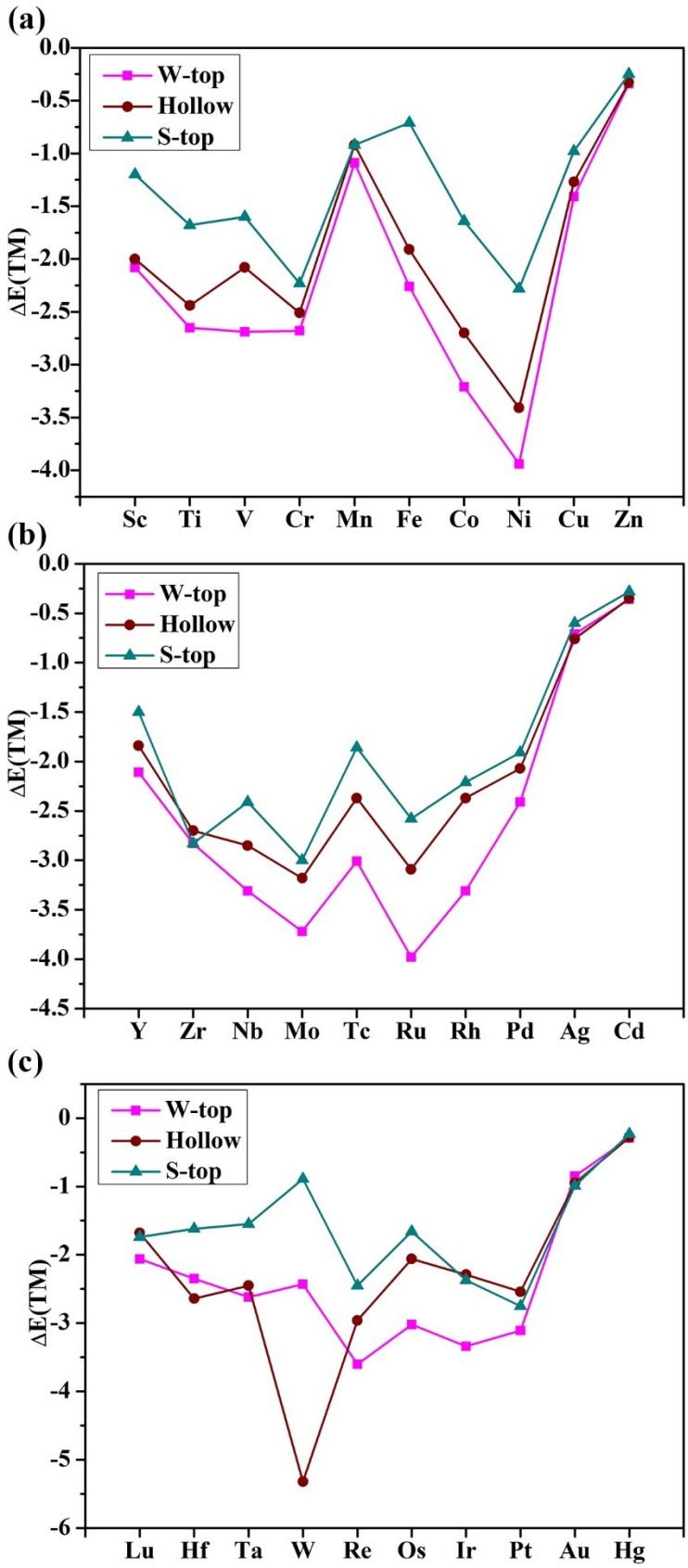

Figure S4. The calculated adsorption energy (in eV) of **(a)** 3d, **(b)** 4d, **(c)** 5d TM anchored on WS_2 monolayer at W-top, Hollow and S-top sites.

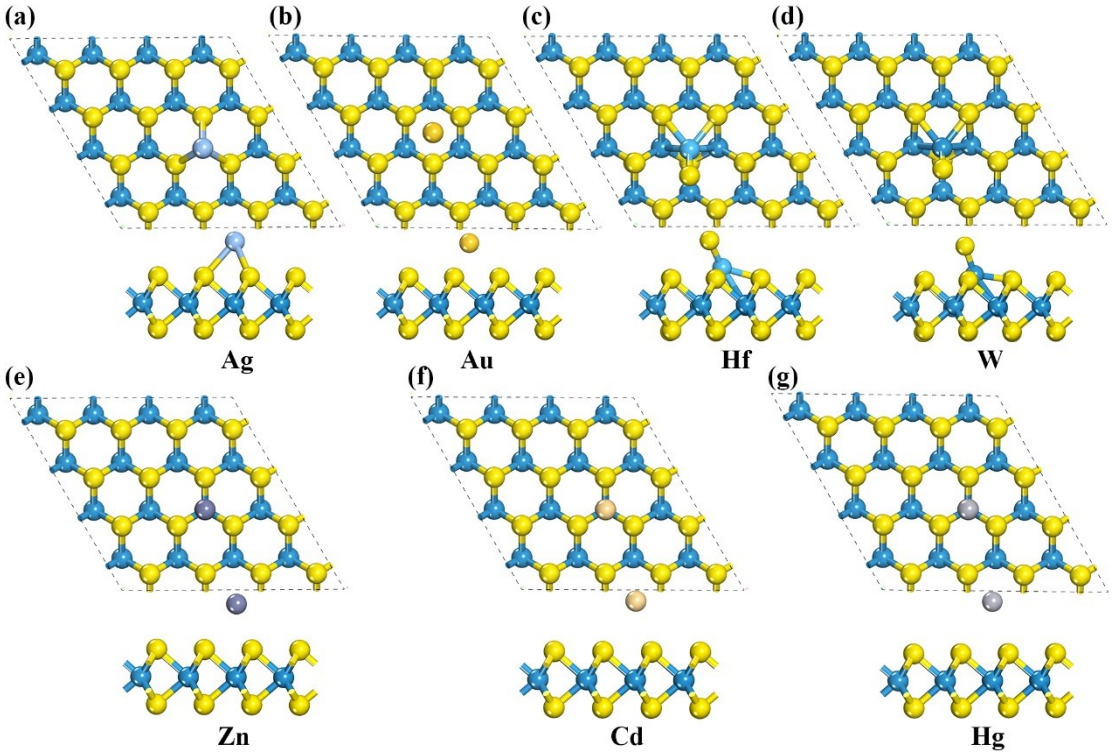

Figure S5. Optimized structure of **(a)** Ag, **(b)** Au, **(c)** Hf, **(d)** W, **(e)** Zn, **(f)** Cd and **(g)** Hg anchored on WS_2 monolayer at the most stable site.

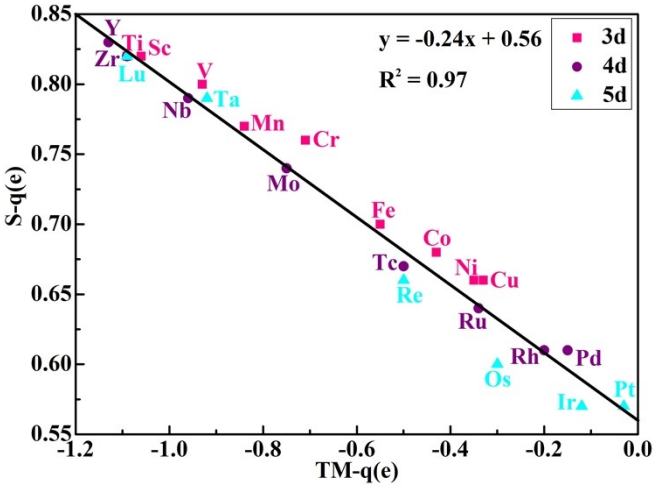

Figure S6. Bader charge of TM and S ligands. Positive and negative values indicate that the atom gains and loses electrons, respectively.

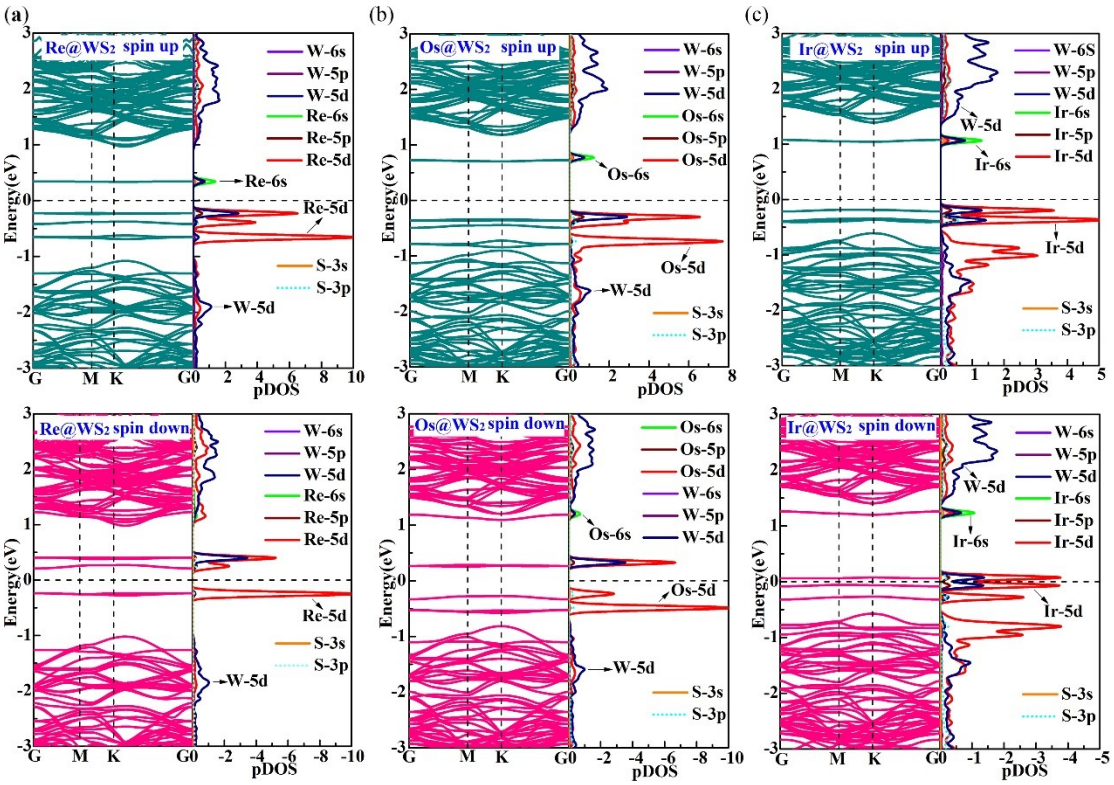

Figure S7. Band structure and PDOS of **(a)** $Re@WS_2$, **(b)** $Os@WS_2$, **(c)** $Ir@WS_2$ for spin-up (the upper picture) and spin-down (the bottom picture) channels.

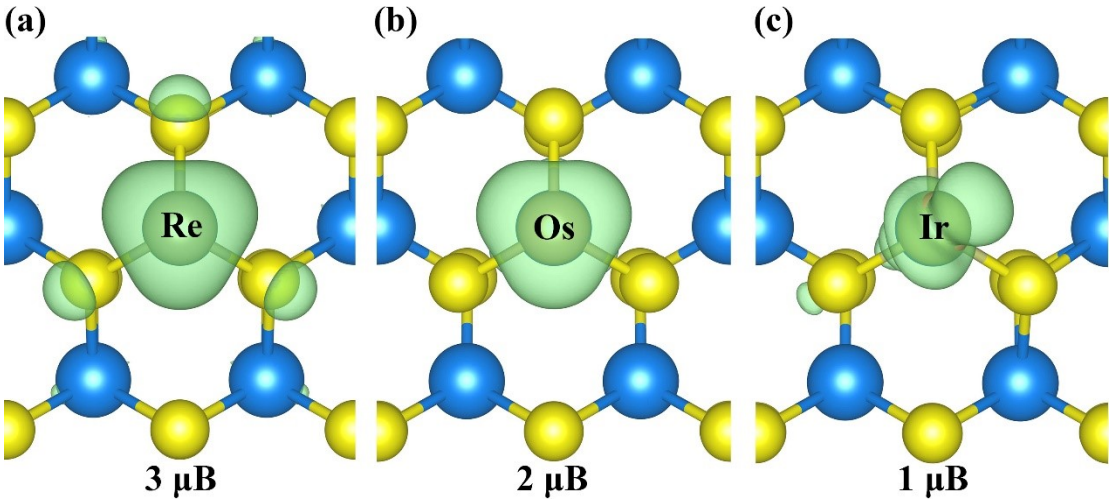

Figure S8. Spin-resolved density of **(a)** $Re@WS_2$, **(b)** $Os@WS_2$ and **(c)** $Ir@WS_2$. The green region is the spin charge clouds (in 0.005 $eÅ^{-3}$). The calculated total spin moment of $Re@WS_2$, $Os@WS_2$ and $Ir@WS_2$ are 3 μB, 2 μB and 1 μB, respectively.

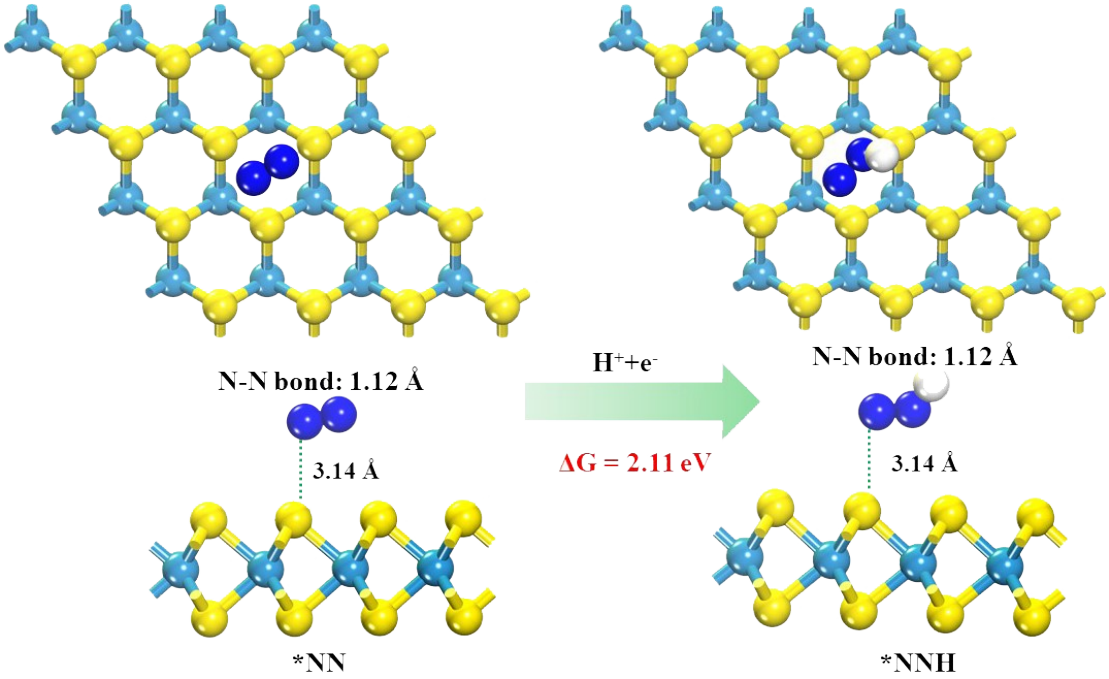

Figure S9. The free energy change of the first hydrogenation (*NN→*NNH) on the pristine WS_2 monolayer. The extremely positive free energy change indicates that the pristine WS_2 monolayer has no catalytic activity for NRR.

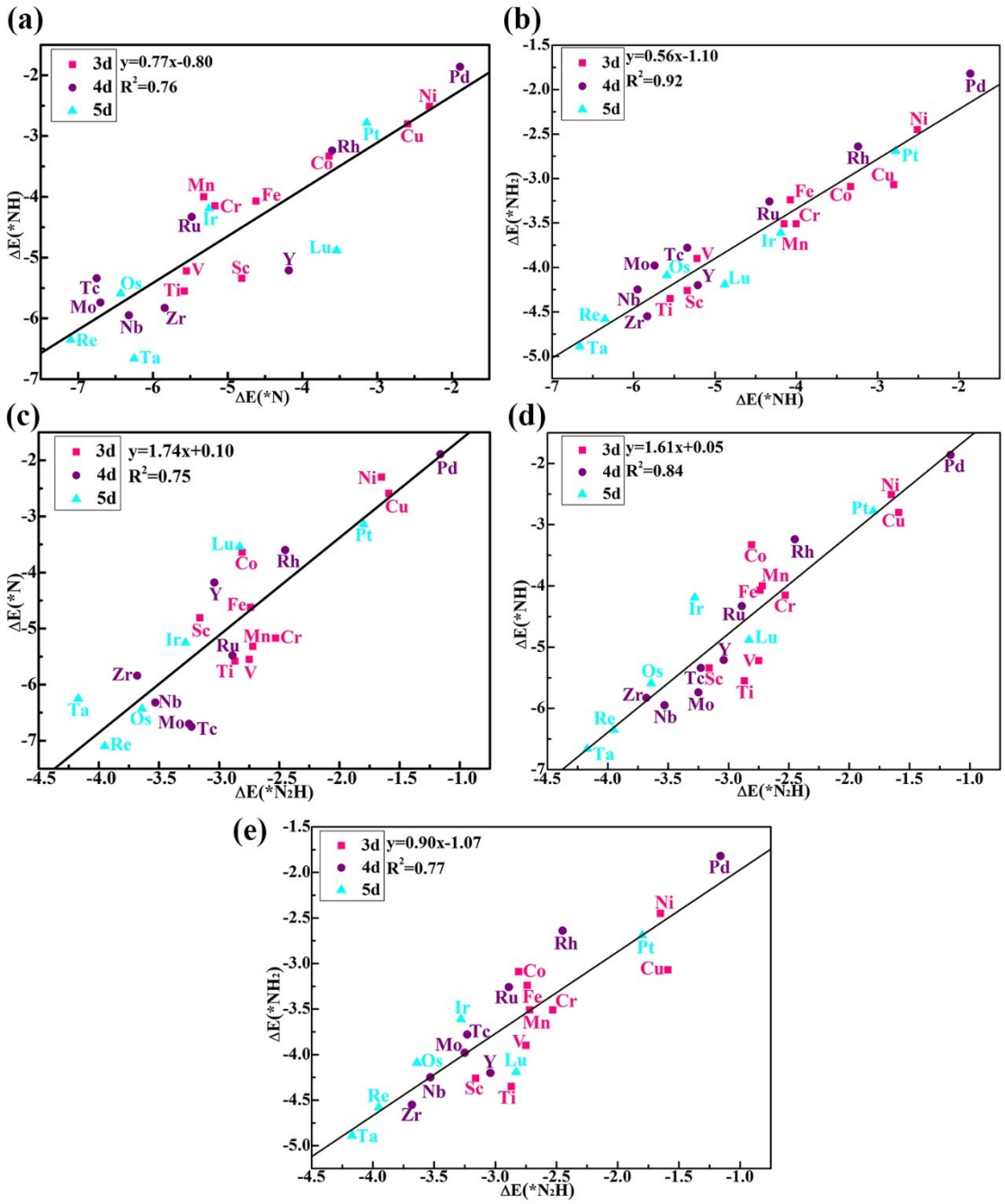

Figure S10. Linear scaling relationship between the adsorption energies of reaction intermediates **(a)** *N vs *NH, **(b)** *NH vs *NH_2, **(c)** *N_2H vs *N, **(d)** *N_2H vs *NH, **(e)** *N_2H vs *NH_2.

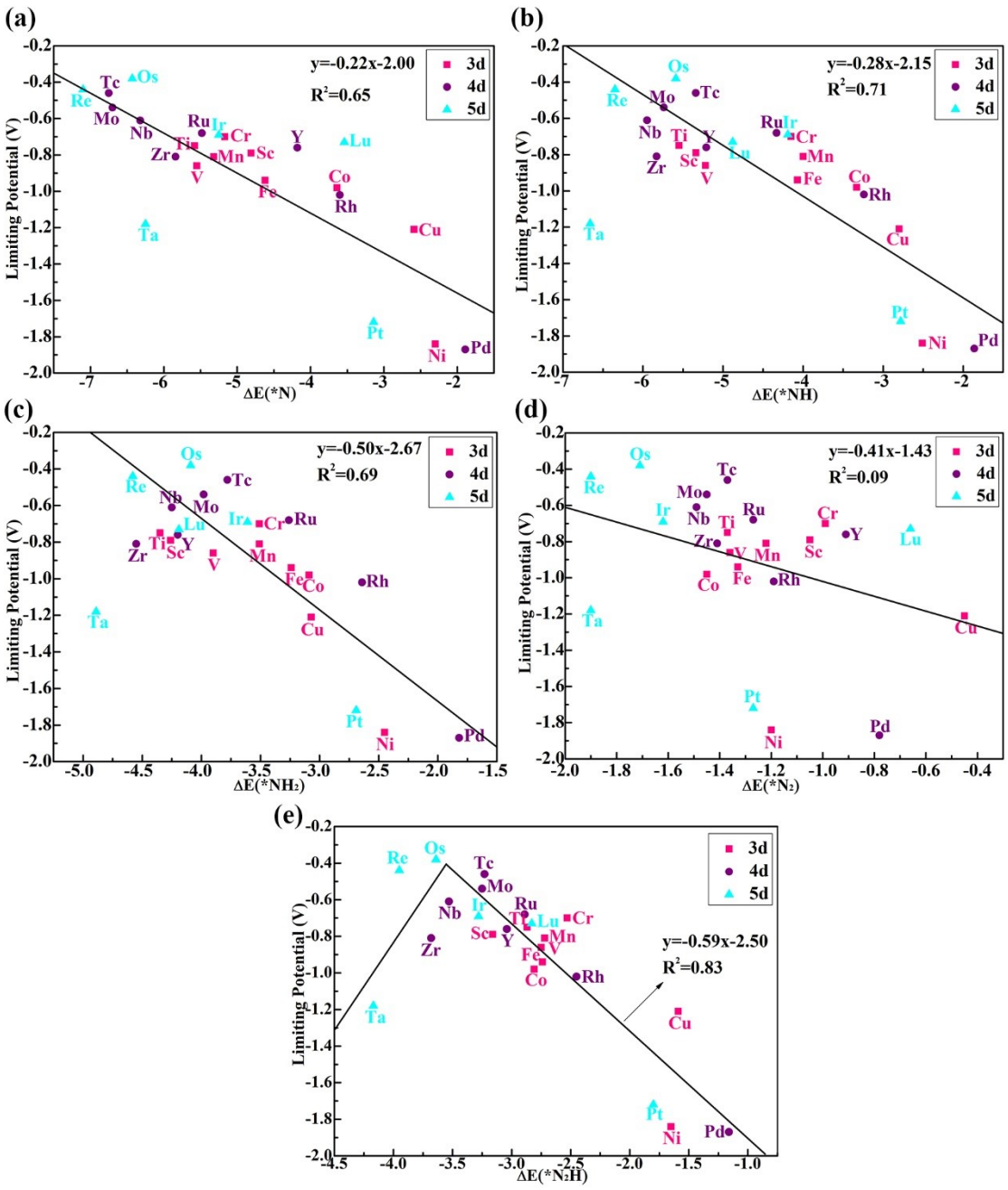

Figure S11. The correlation between the U_L of NRR and **(a)** ΔE(*N), **(b)** ΔE(*NH), **(c)** ΔE(*NH_2), **(d)** ΔE(*N_2), **(e)** ΔE(*N_2H).

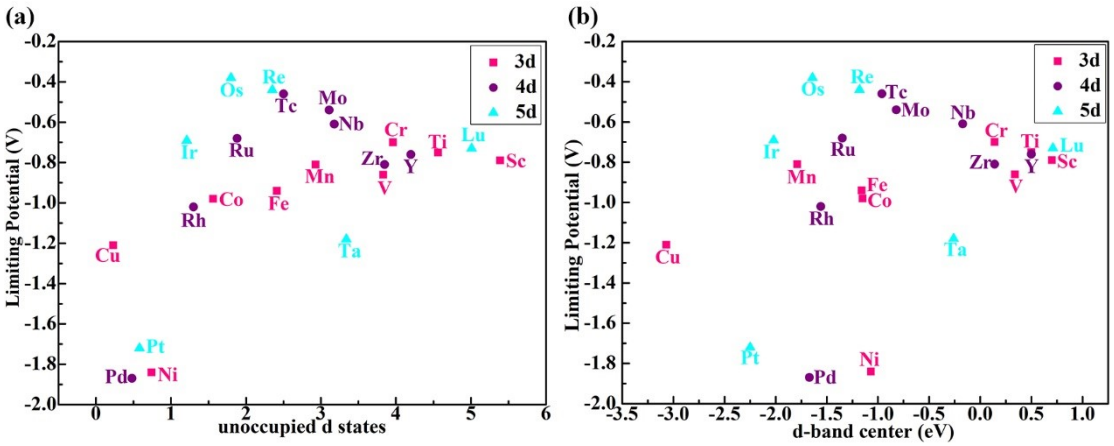

Figure S12. Scatter plots of **(a)** the unoccupied d states and the U_L of NRR, **(b)** the d-band center and the U_L of NRR. The unoccupied d states are obtained by integrating the electronic density of states with respect to energy above the Fermi level. The d-band center is calculated by the formula:

$$\varepsilon_d = \frac{\int_{-\infty}^{\infty} n_d(\varepsilon)\varepsilon \, d\varepsilon}{\int_{-\infty}^{\infty} n_d(\varepsilon) \, d\varepsilon}$$

; where $n_d(\varepsilon)$ is the electronic density of states of d-states and ε is energy.

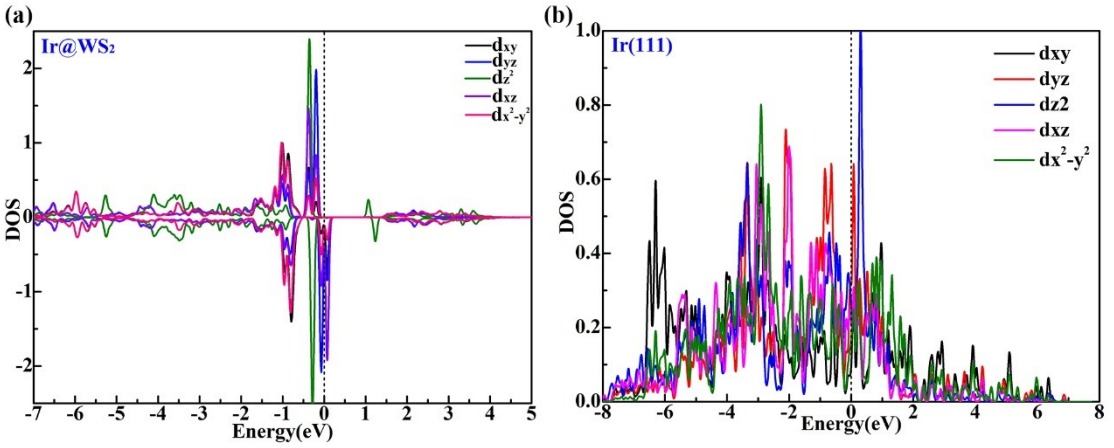

Figure S13. The PDOS of **(a)** Ir SAC and **(b)** Ir(111) are taken as examples to illustrate the difference between d bands of TM SACs and TM surfaces.

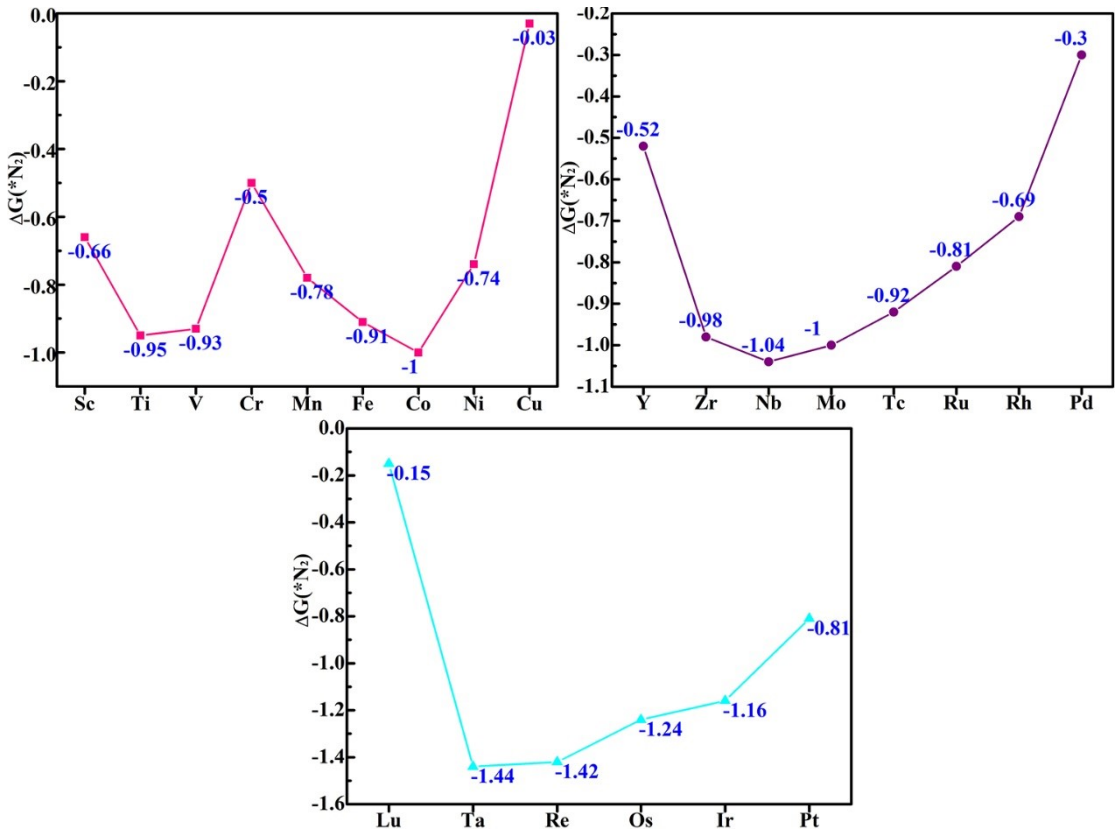

Figure S14. The adsorption Gibbs free energy of N_2 on TM@WS_2 in the form of the most stable coordinated mode (end-on or side-on). $\Delta G(*N_2) = G(N_2\text{-TM@}WS_2) - G(\text{TM@}WS_2) - G(N_2)$, where $G(N_2\text{-TM@}WS_2)$, $G(\text{TM@}WS_2)$ and $G(N_2)$ represent the Gibbs free energies of N_2 adsorption system, substrate and free N_2, respectively.

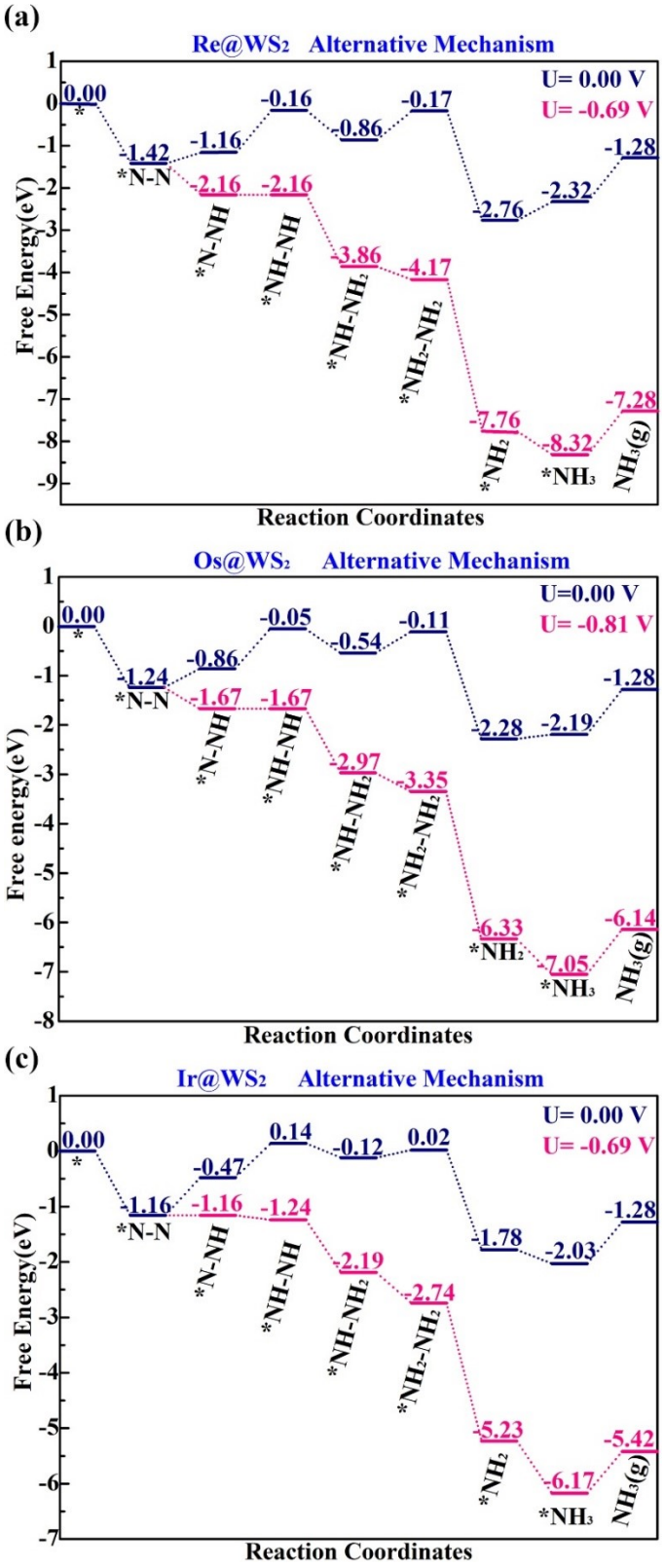

Figure S15. Free energy diagrams of NRR on **(a)** Re@WS_2, **(b)** Os@WS_2, **(c)** Ir@WS_2 via alternative pathway. The data marked in pink indicate situations where the applied electrode potential for electrocatalytic reaction is not zero.

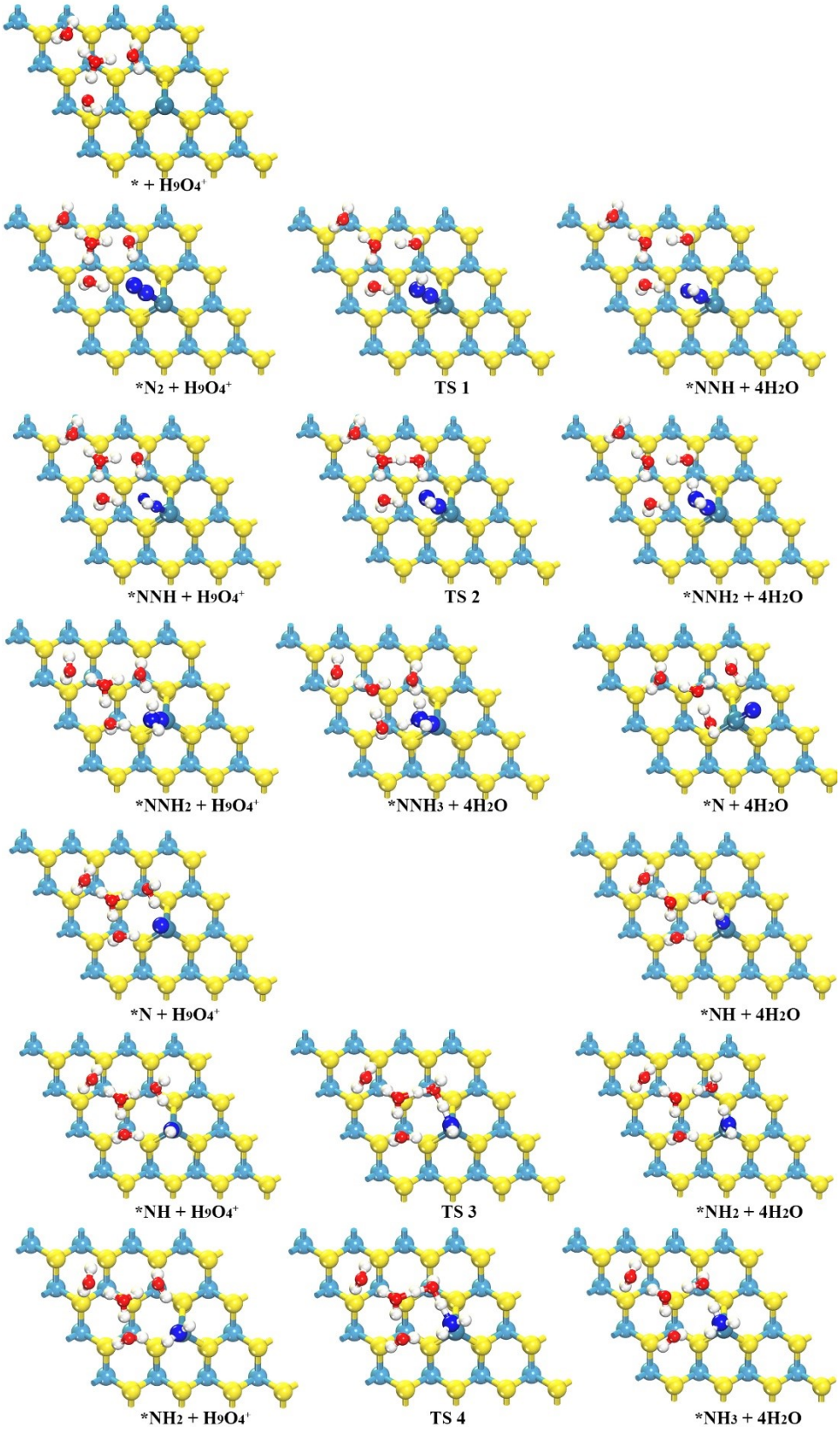

Figure S16. The atomic structures of initial states, intermediates, transition states (TS) and final states on Re@WS_2. TS is searched by using CI-NEB method. The geometric structures of initial states, final states, intermediates are fully relaxation.

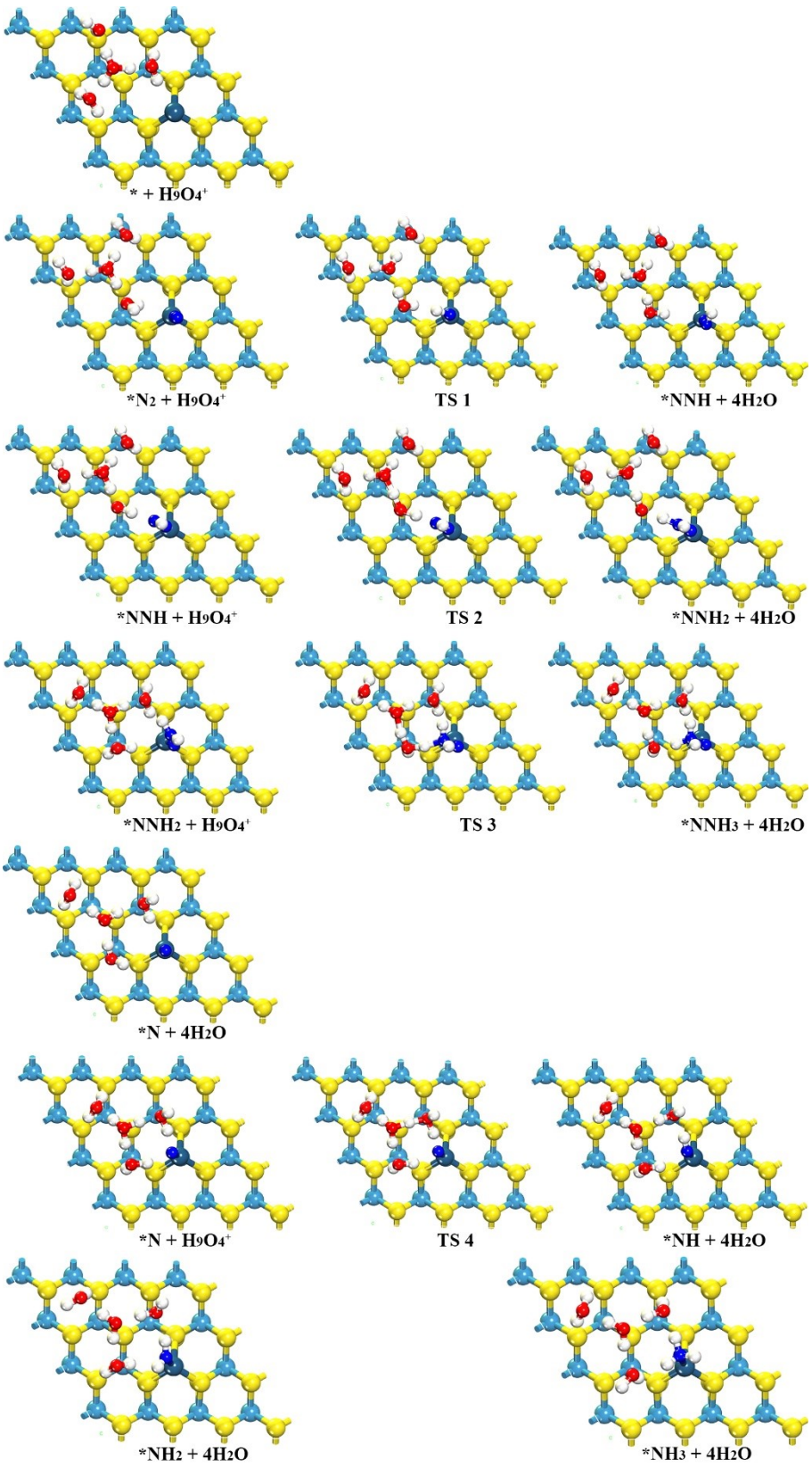

Figure S17. The atomic structures of initial states, intermediates, transition states (TS) and final states on Ir@WS_2. TS is searched by using CI-NEB method. The geometric structures of initial states, final states, intermediates are fully relaxation.

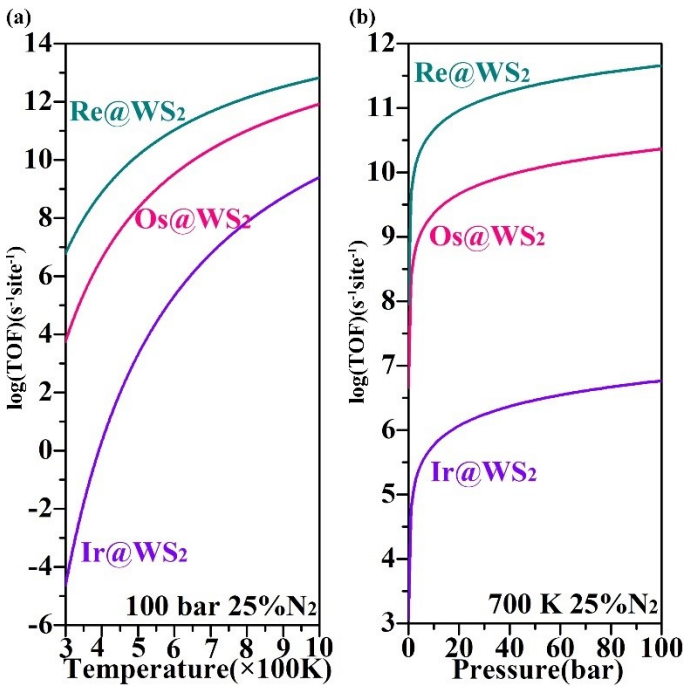

Figure S18 (a) The curve of TOF with temperature at 100 bar. **(b)** TOF as a function of pressure at 700 K.

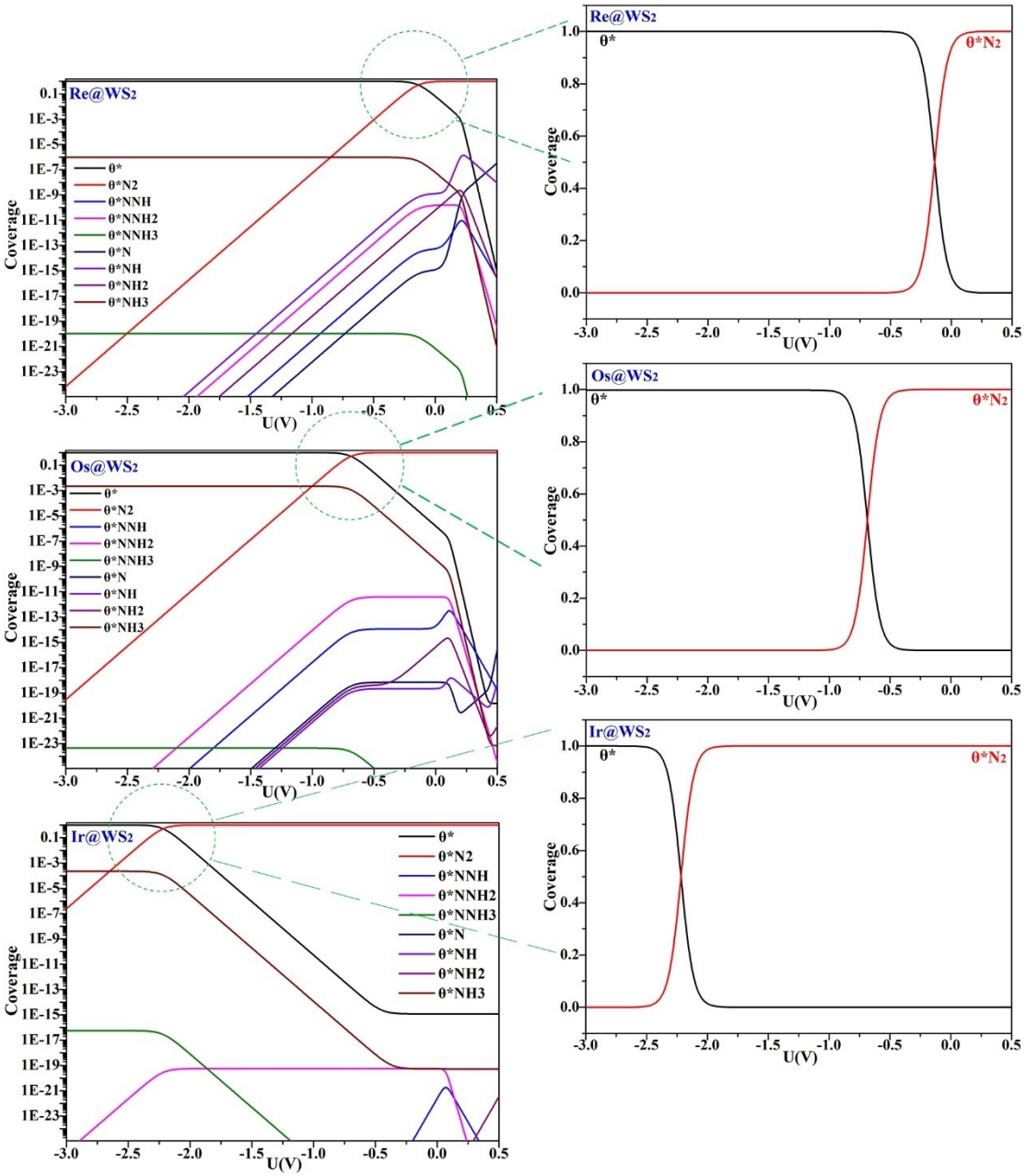

Figure S19. The coverages (θ) of intermediates as a function of the electrode potential (U in V) at 298.15 K.

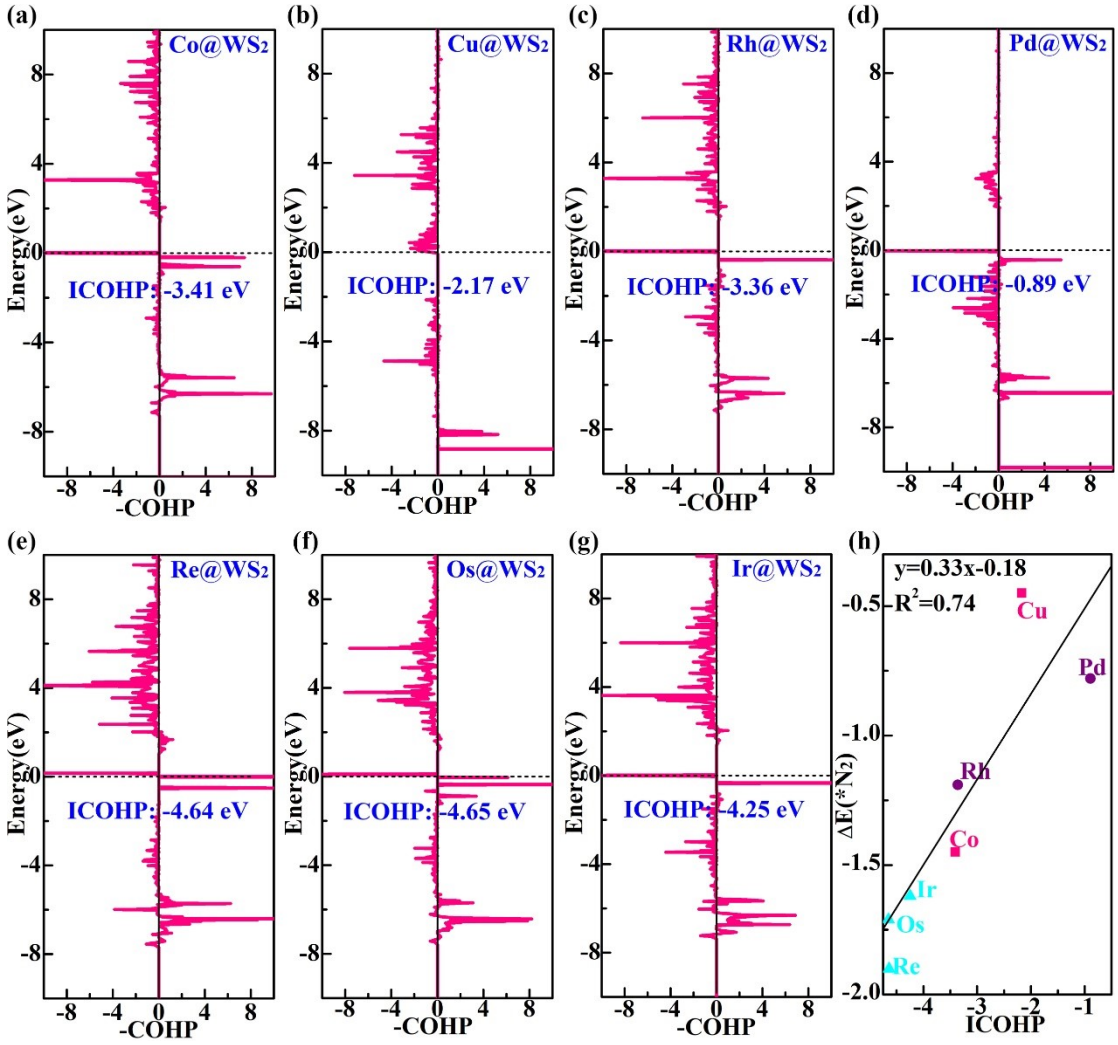

Figure S20. Crystal orbital Hamilton population (COHP) between the TM center from **(a)** Co to **(g)** Ir and the proximal N of the adsorbed N_2 molecule. **(h)** The linear relation between integrated COHP (ICOHP) and the adsorption energy of N_2 molecule ($\Delta E(*N_2)$). Positive and negative values of –COHP indicate bonding and antibonding contributions, respectively. The Fermi level (E_F) is represented by horizontal dashed line.

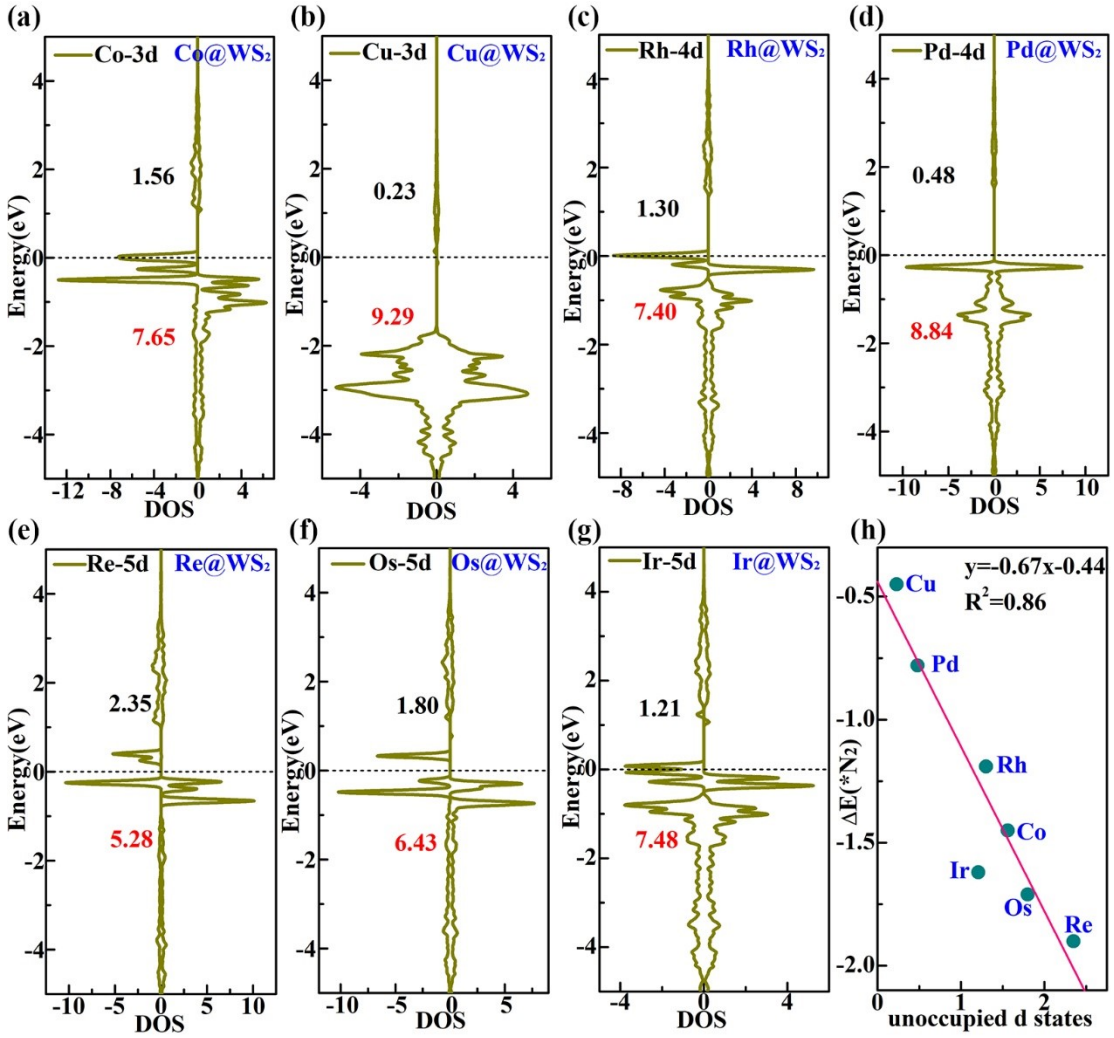

Figure S21. PDOS of **(a)** Co, **(b)** Cu, **(c)** Rh, **(d)** Pd, **(e)** Re, **(f)** Os, **(g)** Ir in the TM@WS_2 system. **(h)** The linear relation between the unoccupied d states and the adsorption energy of N_2 molecule ($\Delta E(*N_2)$). The Fermi level (E_F) is set to zero. The red number to below the E_F indicates the occupied d states and the black number above the E_F suggests the unoccupied d states.

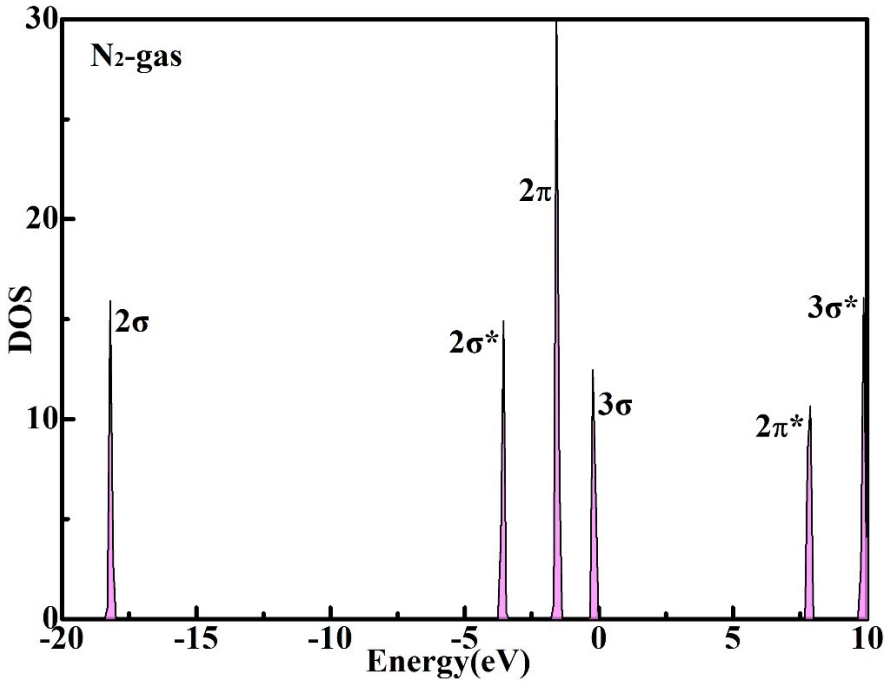

Figure S22. Molecular orbitals of gaseous N_2.

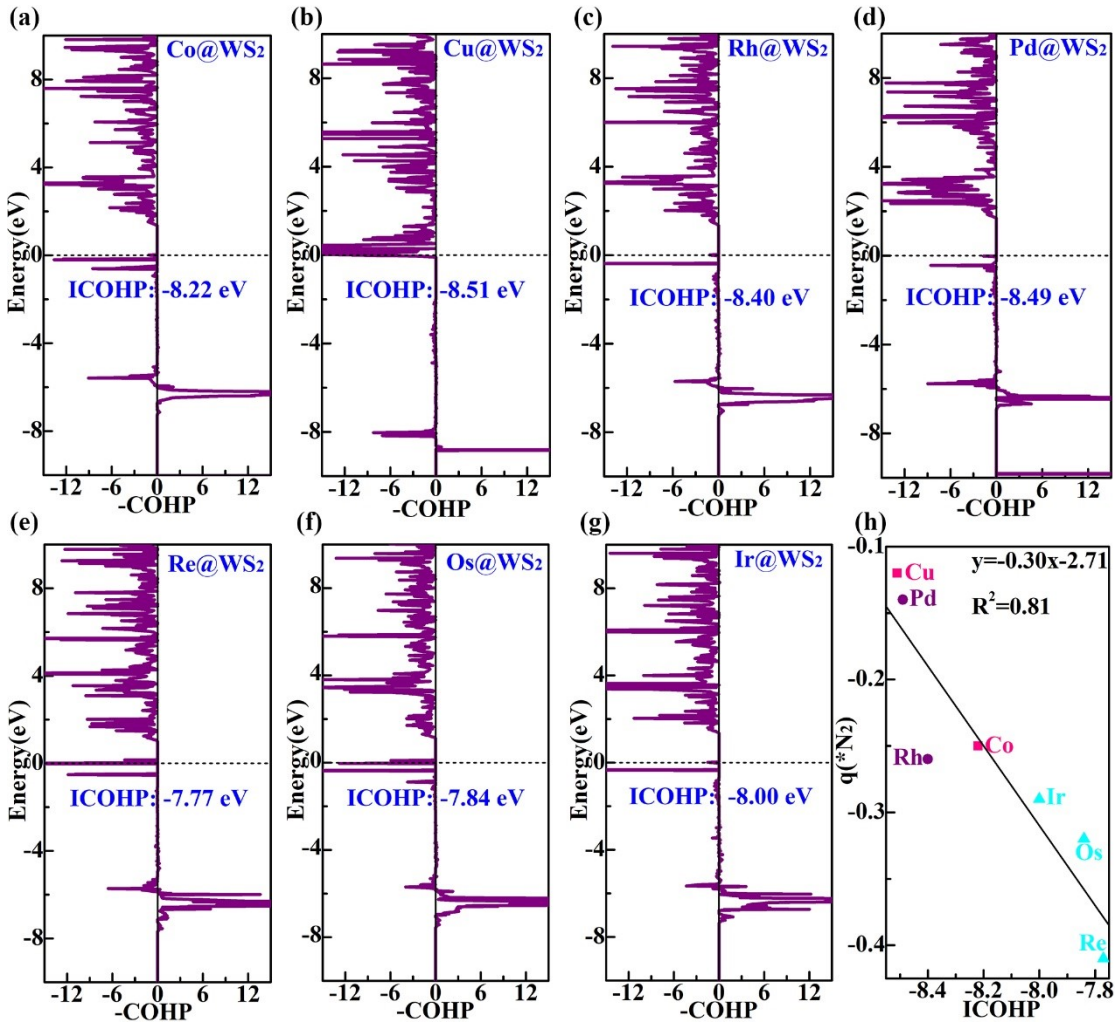

Figure S23. Crystal orbital Hamilton population (COHP) of the N≡N bond in **(a)** Co@WS_2, **(b)** Cu@WS_2, **(c)** Rh@WS_2, **(d)** Pd@WS_2, **(e)** Re@WS_2, **(f)** Os@WS_2 and **(g)** Ir@WS_2 with N_2 adsorption. (**h**) The linear relation between ICOHP of the N≡N bond and the charge state of adsorbed N_2 (q(*N_2)). A negative charge state of *N_2 indicates N_2 gains electrons upon the adsorption process. Positive and negative values of –COHP indicate bonding and antibonding contributions, respectively. The Fermi level (E_F) is represented by horizontal dashed line.

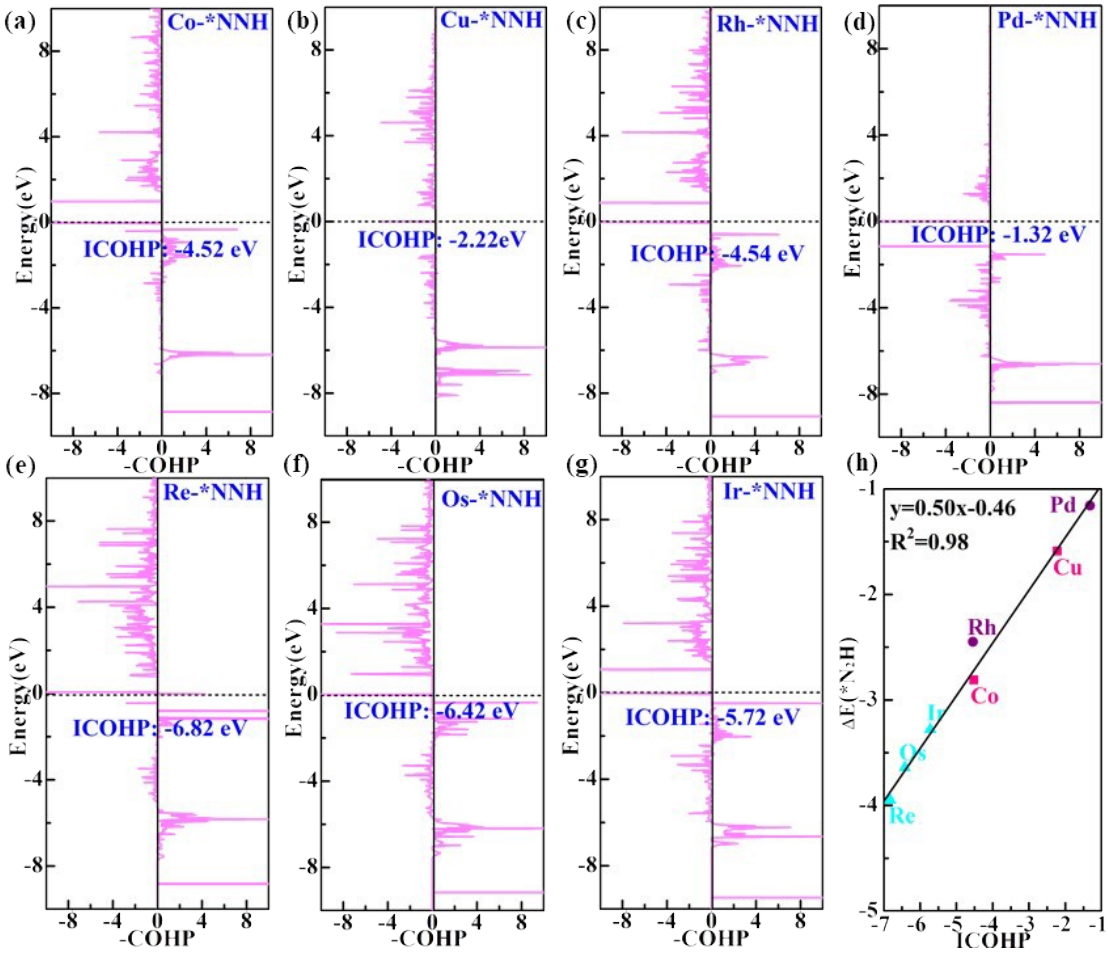

Figure S24. Crystal orbital Hamilton population (COHP) of the TM-N bond in **(a)** Co@WS_2, **(b)** Cu@WS_2, **(c)** Rh@WS_2, **(d)** Pd@WS_2, **(e)** Re@WS_2, **(f)** Os@WS_2 and **(g)** Ir@WS_2 with N_2H adsorption. (**h**) The linear relation between ICOHP of the TM-N bond and the adsorption energies of adsorbed N_2H ($\Delta E(*N_2H)$). Positive and negative values of –COHP indicate bonding and antibonding contributions, respectively. The Fermi level (E_F) is represented by horizontal dashed line.

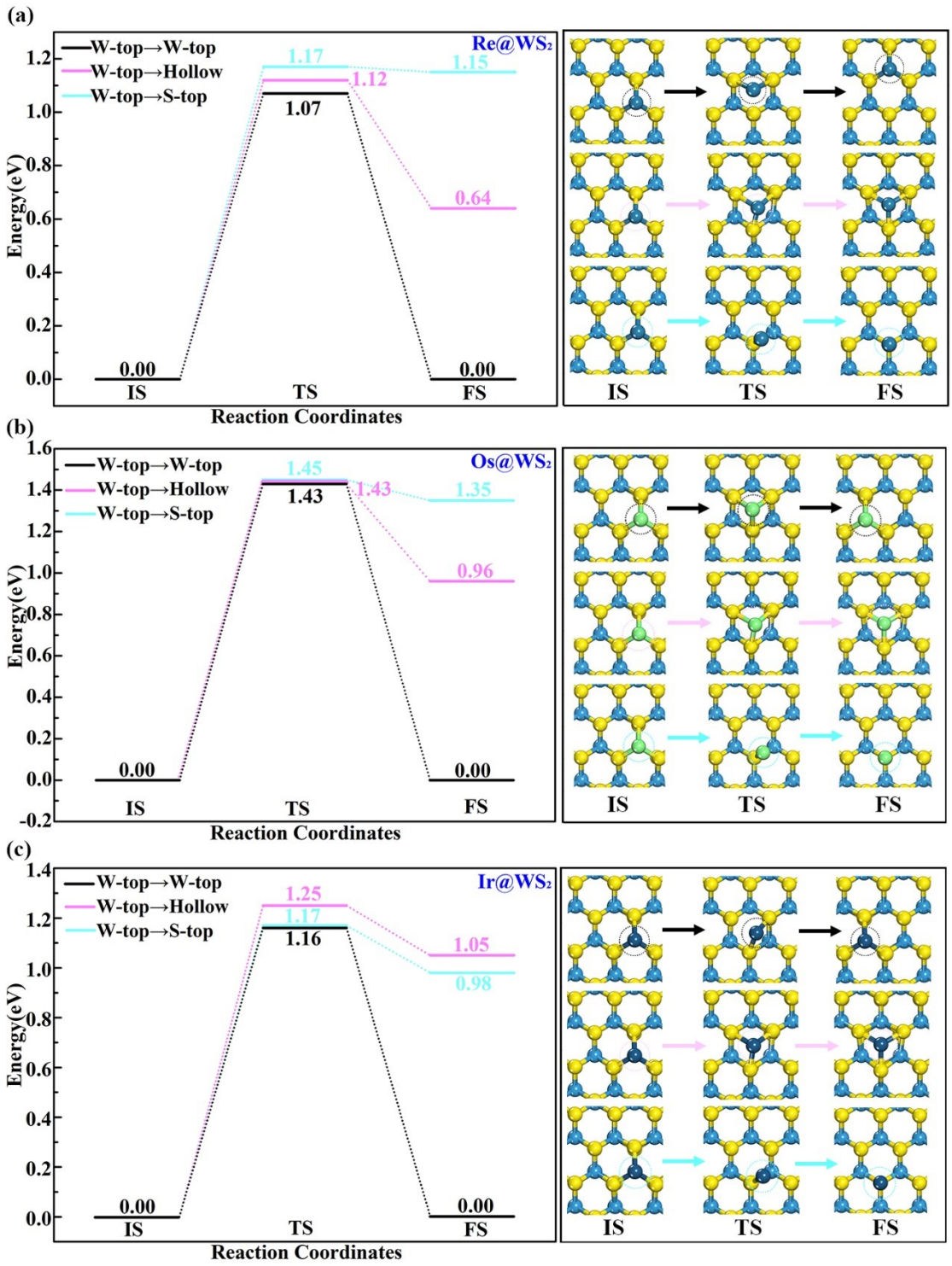

Figure S25. Energy barrier of **(a)** Re, **(b)** Os, **(c)** Ir diffusion via three migration pathways, i.e., the TM diffusion from the W-top site to the adjacent W-top site (black line) or from the W-top site to the Hollow site (pink line) or from the W-top site to the S-top site (cyan line). IS, TS, FS represent the initial state, transition state, final state.

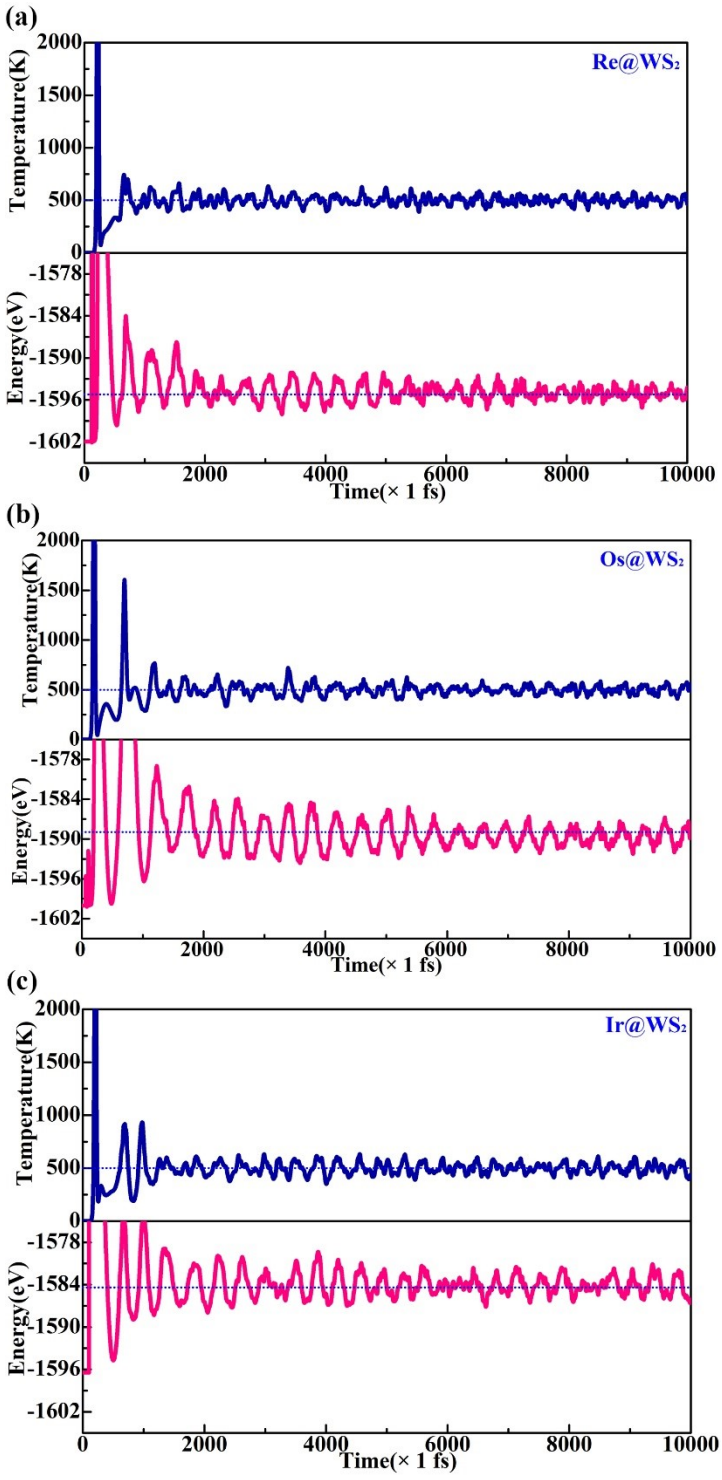

Figure S26. Ab initio molecular dynamics (AIMD) simulation of **(a)** Re@WS_2, **(b)** Os@WS_2, **(c)** Ir@WS_2 at 500 K. A canonical ensemble (NVT) is simulated using the algorithm of Nosé and the time step is 1 fs.

References:

1 X. Liu, X. Lv, P. Wang, Q. Zhang, B. Huang, Z. Wang, Y. Liu, Z. Zheng and Y. Dai, *ELECTROCHIM ACTA*, 2020, **333**, 135488.

2 W. Zhao, L. Zhang, Q. Luo, Z. Hu, W. Zhang, S. Smith and J. Yang, *ACS CATAL*, 2019, **9**, 3419-3425.

3 X. Liu, Y. Jiao, Y. Zheng, M. Jaroniec and S. Qiao, *J AM CHEM SOC*, 2019, **141**, 9664-9672.

4 N. Marcella, J. S. Lim, A. M. Płonka, G. Yan, C. J. Owen, J. E. S. van der Hoeven, A. C. Foucher, H. T. Ngan, S. B. Torrisi, N. S. Marinkovic, E. A. Stach, J. F. Weaver, J. Aizenberg, P. Sautet, B. Kozinsky and A. I. Frenkel, *NAT COMMUN*, 2022, **13**.

5 C. Choi, G. H. Gu, J. Noh, H. S. Park and Y. Jung, *NAT COMMUN*, 2021, **12**.

6 Q. Wu, H. Wang, S. Shen, B. Huang, Y. Dai and Y. Ma, *Journal of materials chemistry. A, Materials for energy and sustainability*, 2021, **9**, 5434-5441.

7 H. Zhang, S. Wang, H. Wang, B. Huang, S. Dong, Y. Dai and W. Wei, *NANOSCALE*, 2021, **13**, 17331-17339.

8 X. Mao, Z. Gu, C. Yan and A. Du, *J MATER CHEM A*, 2021, **9**, 6575-6582.

9 G. Kour, X. Mao and A. Du, *J MATER CHEM A*, 2022, **10**, 6204-6215.

10 S. Zhou, X. Yang, X. Xu, S. X. Dou, Du Y and J. Zhao, *J AM CHEM SOC*, 2020, **142**, 308-317.

11 X. Lv, W. Wei, H. Wang, F. Li, B. Huang, Y. Dai and T. Jacob, *J MATER CHEM A*, 2020, **8**, 20047-20053.

12 J. C. Liu, X. L. Ma, Y. Li, Y. G. Wang, H. Xiao and J. Li, *NAT COMMUN*, 2018, **9**, 1610.

13 Y. Wang, Y. J. Tang and K. Zhou, *J AM CHEM SOC*, 2019, **141**, 14115-14119.

14 H. A. Hansen, V. Viswanathan and J. K. Nørskov, *The Journal of Physical Chemistry C*, 2014, **118**, 6706-6718.